

# SLM of Al-Based Matrix Composites

Subjects: Materials Science, Composites

Contributor: Ivan Pelevin

Aluminum matrix composites (AMC) are of great interest and importance as high-performance materials with enhanced mechanical properties. Al<sub>2</sub>O<sub>3</sub> is a commonly used reinforcement in AMCs fabricated by means of various technological methods, including casting and sintering. Selective laser melting is a suitable modern method of the fabrication of net-shape fully dense parts from AMC with alumina.

Keywords: metal matrix composites ; selective laser melting ; aluminum matrix composites ; mechanical properties ; alumina ; laser powder bed fusion ; aluminum alloys

---

## 1. Background

Metal matrix composites (MMCs) have become widely used as construction materials, among which Al-based MMCs are employed for highly demanding applications such as in aircraft and automotive industries, as well as the military [1][2][3][4][5][6][7]. The introduction of reinforcing particles into the metallic matrix is the admitted approach of economical materials production [8][9][10].

Superior mechanical properties, particularly high strength-to-weight ratios, ductilities, moduli, excellent wear and corrosion resistances, and creep resistances at elevated temperatures, could be obtained [5][11][12]. Parts of engines and pistons, etc. require superior tribological properties of the materials from which they are made, making aluminum matrix composites (AMCs) with Al<sub>2</sub>O<sub>3</sub> or SiC reinforcing particles suitable for such applications [13][14][15][16][17][18][19][20][21][22]. The presence of the alumina particulates partially taking on external loads and exhibiting good bonding properties with the Al matrix provides an elevated wear resistance of the composite [23][24][25]. The feature to be considered as a rule is the reduced elongation of the composite [26][27][28]. Among reinforcements, Al<sub>2</sub>O<sub>3</sub> benefits from its stability at elevated temperatures and dissolving into Al with no undesirable phase formations [29].

The aluminum alloy composites can be produced via various synthesis approaches [2][30], involving casting [31][32] and stir casting [5][33], which are characterized by a strong particle bonding, matrix structure control simplicity, and near-net-shape, as well as being one of the most economical [2][30][34][35][36]. These technological routes imply the addition of reinforcing particles into a molten matrix, and the main problems associated with casting processes are the achievements of sufficient wettability and a reinforcement phase heterogeneous distribution [33]. The difference between particles and matrix density leads to particles floating or sinking, thus causing a nonuniform dispersion [37][38][39][40]. If the density of alumina (3.97 g/cm<sup>3</sup>) is higher than that of aluminum (2.7 g/cm<sup>3</sup>), the sinking of particles is observed. The mixing of the matrix and ceramic particles in the solid state within powder metallurgy methods with subsequent sintering is considered the most widely used technique for aluminum alloy composites [4][41][42]. It allows the achievement of a better microstructure control with a more homogeneous reinforcement distribution. A significant difference in the melting points and compressive strength of alumina and aluminum interrupts the good rearrangement of the particles and leads to porosity, further complicating the Al-Al<sub>2</sub>O<sub>3</sub> fabrication. It was observed that increasing alumina particle size leads to a higher porosity, whereas its decrease provides a higher hardness and tensile strength of the composite [4][5], which is attributed to a greater Al-Al<sub>2</sub>O<sub>3</sub> interfacial area and to a higher likelihood of the fracture of large alumina particles [43]. The complex, expensive, and time- and energy-consuming routes such as mechanical alloying and diffusion bonding [36][44][45] are not considered in this review, because of their rare use. The common problems of all the methods include porosity and the emergence of particle clusters [33][46], which could drastically decrease the mechanical properties.

The modern approach for the fabrication of alloys and MMC includes Al-based composites, particularly selective laser melting (SLM)/laser powder bed fusion (LPBF) [21][47][48][49][50][51][52][53], which implies the layer-by-layer synthesis of powder material according to the computer-aid-designed (CAD) sliced model and provides the manufacturing of net-shape parts. As ceramic particle-reinforced composites are difficult to machine [5], applying near-net-shape production techniques are required, making SLM suitable and promising in relation to Al-based alloy composites with Al<sub>2</sub>O<sub>3</sub> reinforcing.

SLM is characterized by the following set of main parameters:

- $P$ —laser power, W;
- $V$ —scanning speed, mm/s;
- $t$ —layer thickness,  $\mu\text{m}$ ;
- $h$ —hatch spacing,  $\mu\text{m}$ .

Some more specific parameters, e.g., laser spot diameter and profile, substrate heating, and scanning strategy, result in the following sets of energy density (ED):

$$LED = \frac{P}{V} \quad (1)$$

where LED is the linear ED.

$$ED_a = \frac{P}{Vh} \quad (2)$$

where  $ED_a$  is the aerial ED.

$$ED_V = \frac{P}{Vht} \quad (3)$$

where  $ED_V$  is the volume ED.

ED is a simple way for the elementary comparison of different SLM regimes being useful and suitable, especially within working with specific SLM machines. A comparison of Eds used on different SLM machines should be made with the machines' features considered.

In relation to MMC and taking into account those discussed above, the SLM approach has advantages due to its melting peculiarities. The small size of the molten pool, the extremely short lifetime of the liquid state, and, thus, the rapid heating and cooling rates are inherent in the SLM procedure. Therefore, superfine microstructures are usually obtained, which, in turn, leads to a higher strength and hardness according to a dispersion hardening mechanism and Hall–Petch theory [54] [55] [56] [57] [58] [59]. Moreover, the finer reinforcement powder is used in the shorter distance between the reinforcing particles in the material, creating more barriers for the movement of dislocations [54]. Thus, the uniform reinforcing particle distribution is still needed to be achieved after the SLM process. The problem of ceramic particles segregation arises because of their rejection by the solid–liquid interface during solidification [5] [60]. As the size of the molten pool is small and the cooling rates during SLM are extremely high, the particle segregation tendency would be not so significant. Moreover, this problem could almost be solved via SLM if laser irradiation produces an intensive melt flow [61], providing a uniform dispersion of ceramic particles subject to optimal SLM parameters. In addition, the direct impact of laser irradiation and the intensive heating of the small amount of powder material leads to enough heating of both aluminum and alumina particles, improving the wettability of the latter by the liquid Al matrix [62] and enhancing the bonds at the interface [29].

Generally, all the problems that also arise during the SLM process, namely, wettability, the heterogeneous distribution of particles, porosity, and the agglomeration particles, could be overcome by the thorough selection of SLM parameters and the initial mixing regime of powder materials. In summary, SLM combines the advantages of both PM and casting methods; thus, a thorough consideration of this method applied to Al–Al<sub>2</sub>O<sub>3</sub> composites is of current scientific and technological interest.

## 2. Initial Powder Preparation

Mechanical alloying as a solid-state powder processing technique has attracted research interest [63] to prepare initial mixed Al–Al<sub>2</sub>O<sub>3</sub> powder by means of ball-milling with a ball-to-powder weight ratio of 10:1 and the following regime: 16 h of milling with an interval of 10 min after each 30 min of milling. The ball-milling technique has some indisputable advantages applied to thorough mixing and milling, with repeated deformation, fracturing, and cold-welding providing the transfer of mass between components and a uniform distribution in the reinforcement case [64]. However, it should be noted that the application of intensive mechanical milling (ball milling) leads to numerous problems for subsequent selective laser

melting. Namely, the milling of initial powder with a spherical morphology inevitably spoils the sphericity of the particles regardless of the ball-to-powder ratio, rotation speed, powder properties, particle size, etc. Moreover, the agglomeration and aggregation of particles with the expansion of particle size distribution during milling occurs especially in the case of nanosized particles [65]. Despite the suggestions in [63], all these could significantly decrease the powder flowability, which is of great importance in the formation of each layer during the SLM procedure, making the preparation of suitable composite powders challenging [66]. It is known [20][67] that a low flowability and sphericity, along with a wide particle size distribution, negatively affects selective laser melting, causing a decrease in powder bulk density, and resulting in a high porosity of the printed material. Another undesirable effect of ball milling that usually occurs is powder contamination (by iron, as a rule) of the material as a result of the abrasion and destruction of balls and camera walls [64]. Another peculiarity of the feedstock powder morphology in [63] is the ratio of the initial Al and Al<sub>2</sub>O<sub>3</sub> particle size: an Al average particle size an order smaller than that of alumina, which is not typical for powders for the fabrication of metal matrix composites by means of any technique. The final particle size of Al<sub>2</sub>O<sub>3</sub> particles after milling was significantly refined but remained more than twice as large. The features of this work [63] mentioned above could make a significant impact on the microstructure and mechanical properties, leaving room for further improvement in the mechanical behavior of Al-Al<sub>2</sub>O<sub>3</sub> composites fabricated by SLM.

Despite that, the ball-milling method is widely used for SLM powder preparation. Han et al. [66][68] investigated ball-milled Al-Al<sub>2</sub>O<sub>3</sub> nanocomposites for SLM applications, and they carried it out with 200 g of Al and 4 vol.% of Al<sub>2</sub>O<sub>3</sub> powders with a 5:1 ball-to-powder weight ratio. Unlike Jue et al., the Al<sub>2</sub>O<sub>3</sub> particle size in [66][68] was far less (<50 nm). Undesirable processes such as cold-welding or oxidation that are usually observed during ball-milling require special approaches. Han et al. offered the addition of stearic acid to prevent the cold-welding of the material and iron from the grinding bowl and balls, and the filling of the grinding bowls with argon gas to avoid oxidation. However, obtaining a high sphericity of the powder particles after ball-milling is still impossible, which, again, proved the powder images in the studies by Han et al. They also made a similar conclusion to Jue et al. about the combination of the milling for 10 min with pauses for 15 min in order to obtain a narrow particle distribution. It is well known [69][70][71][72][73][74][75] that achieving a proper mixing of nano-sized powders is challenging because of the tendency of the nanoparticles to agglomerate due to van der Waals forces. That is why the handling of nanopowders using simple mixing methods, for example, a tilting drum blender, is not applicable and needs more complex approaches, one of which is ball-milling. Du et al. [76] also reported the preparation of Al-based composites with 2 and 5 wt.% of nano-sized Al<sub>2</sub>O<sub>3</sub> for SLM. Gas-atomized AlSi10Mg powder with normally distributed particles from 20 to 63 μm with a mean diameter of 42 μm was successfully mixed with the nano-sized nAl<sub>2</sub>O<sub>3</sub> reinforcement powder (nominal diameter of 270 nm) by means of ball-milling for 5 h at 600 rpm and with a ball-to-powder ratio of 1:1.

The advanced method of aluminum-alumina powder for SLM was proposed in previous studies [77][78][79]. The composite powder was obtained by the oxidation of aluminum in water, resulting in a core-shell aluminum-alumina morphology, wherein the sphericity and particle size distribution remained nearly unchanged, providing a high flowability and bulk density, which is of great importance for the further SLS/SLM process. The alumina content dependence on the temperature of the oxidation process was shown.

Thus, the initial powder morphology could be divided into three main types: particle blends with comparable sizes of metal matrix particles and nonmetal additives; a mixture of nano-sized additives; and a powder of core-shell particles—see [Figure 1](#).

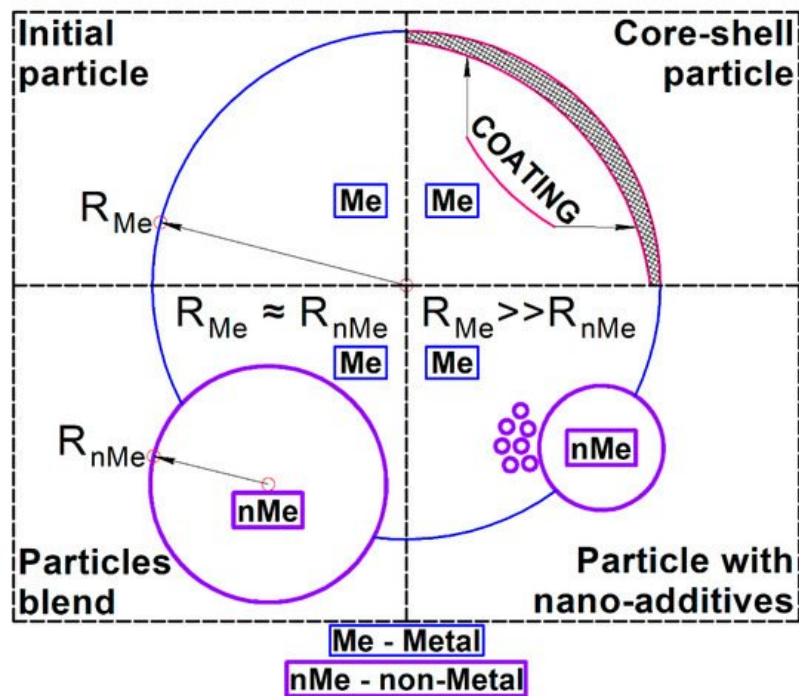


Figure 1. Types of initial powder morphology for SLM of metal-matrix composites with nonmetal additives.

The main features of the initial powder preparation, including the powder morphologies and mixing regimes used in the observed studies, are collected in [Table 1](#).

Table 1. Feedstock powder characterization.

Material	Powder Morphology	Mixing Regime	Reference
Al-Al <sub>2</sub> O <sub>3</sub> 80:20 weight ratio	Al—1.02 μm average particle size; Al <sub>2</sub> O <sub>3</sub> —9.04 μm.	High-energy planetary mono-mill. 16 h with interval of 10 min after each 30 min of milling. 200 rpm.	[63]
AlSi <sub>10</sub> Mg-Al <sub>2</sub> O <sub>3</sub> 80:20 weight ratio	AlSi <sub>10</sub> Mg—gas atomized, 30 μm average particle size; Al <sub>2</sub> O <sub>3</sub> —9.04 μm.	Ball-to-powder weight ratio of 10:1, a rotation speed of 200 rpm, and a milling time of 8 h.	[80][81][82]
Al and 4 vol.% of Al <sub>2</sub> O <sub>3</sub>	Al—17.1 μm average particle size; Al <sub>2</sub> O <sub>3</sub> —10.37 μm.	Ball-to-powder weight ratio of 5:1, 350 rpm, 20 h. Milling of 15 min and pause of 5 min (method 1), milling of 10 min and pause of 15 min combination (method 2)	[66][83][84]
AlSi <sub>10</sub> Mg + 2–5wt.% nanoAl <sub>2</sub> O <sub>3</sub>	AlSi <sub>10</sub> Mg—atomized, 42 μm average particle size; nAl <sub>2</sub> O <sub>3</sub> —270 nm	Single-axis ball milling at 600 rpm, 5 h, ball-to-powder ratio of 1:1 in a volatile solvent	[76]
Al <sub>2</sub> O <sub>3</sub> -AlSi <sub>10</sub> Mg 1:1 weight ratio	AlSi <sub>10</sub> Mg—33.1 μm average particle size; Al <sub>2</sub> O <sub>3</sub> —26.6 μm	Tumbling ball mill, weight ratio of 1:1	[85]
Al <sub>2</sub> O <sub>3</sub> - AlSi <sub>10</sub> Mg 15:85 weight ratio	AlSi <sub>10</sub> Mg—33.1 μm average particle size; Al <sub>2</sub> O <sub>3</sub> —26.6 μm	10:1 ball-to-powder weight ratio. 4 h, 70 rpm.	[86][87]
Al + 10 wt.% Al <sub>2</sub> O <sub>3</sub> core-shell	D <sub>50</sub> = 42 μm with narrow SPAN (D <sub>90</sub> - D <sub>10</sub> )/D <sub>50</sub> = 1.1)	Core-shell Al-Al <sub>2</sub> O <sub>3</sub> powder obtained by hydrothermal oxidation	[78]

### 3. SLM Regimes, Process Window, and Microstructure

The primary definition and optimization of the SLM parameters route for any new material is generally the same and represents a narrowing of the processing parameters window. The ED may change through variations in the laser power  $P$  or scanning speed  $v$ . Laser power has a directly proportional effect on the ED value, whereas the scanning speed has an inverse proportion, i.e., the higher the speed, the lower the energy supplied to the material per unit time. It is also worth noting that a lower temperature of the melting pool implies a poor viscosity of the melt and, hence, a poor wettability of the

previous printed layer and Al<sub>2</sub>O<sub>3</sub> particles suspended in the melt. Overall, too high a scanning speed leads to a discontinuous melting process, forming unmelted regions, pores, and cracks. Therefore, the densification rate of the material after such laser melting will not be high enough.

On the contrary, low scanning speeds increase the heated area and melting pool temperature, possibly leading to its boiling and, in turn, intensive evaporation and spattering. This not only results in pore formation but also causes undesirable chemical and phase transformations, the shrinkage of porosities, and the formation of thermal cracks [63]. In addition, this route of optimization of SLM parameters should be performed not only in new material development cases but also for each SLM machine, because of differences in their characteristics and features. Process windows for the synthesis of Al-Al<sub>2</sub>O<sub>3</sub> composites used in various studies are depicted in Figure 2 as ranges of P–V ratios. Rays of the same P–V ratio indicate the same LED; regions between boundary rays of the same colors indicate the ranges of the used LED in the current research. The overall window includes the wide range of P–V ratios in which the tightly overlapped region is clearly seen. An insufficient laser power as a rule leads to the formation of unmolten defects (lack-of-fusion porosity region in Figure 2). Too slow a scanning speed, in turn, leads to keyhole porosity, while too high an ED initiates the balling effect [88][89], as well as boiling and evaporation of the melt (discussed in detail in Section 4). It does not mean that optimal SLM regimes must lie within the process window; on the contrary, an optimal P–V ratio could even go out of the frame of the overall window shown because of other factors such as powder morphology, layer thickness, hatch spacing, and scanning strategy. All boundaries of the mentioned regions are smooth. However, Figure 2 displays the most possible optimal window that one can focus on to start the optimization of the SLM parameters route. It should be mentioned that although such a direct comparison of the SLM regimes as in Figure 2 is not completely correct, because of other parameters and the difference in machine features, all reviewed research of Al-Al<sub>2</sub>O<sub>3</sub> composites was performed using similar continuous-wave ytterbium fiber lasers of various powers with a TEM<sub>00</sub> laser operation mode [90].

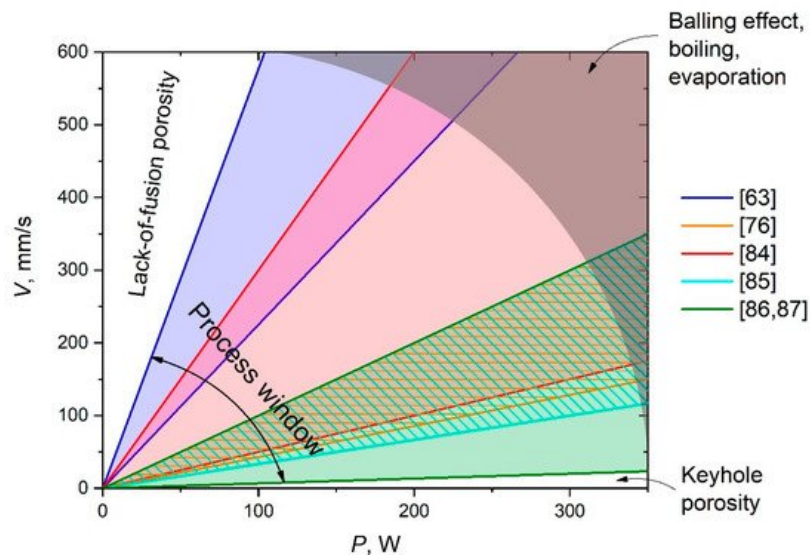


**Figure 2.** P–V diagrams representing process windows for Al-Al<sub>2</sub>O<sub>3</sub> composites synthesis.

Such a route can be clearly seen in a previous study [63] applied to Al-Al<sub>2</sub>O<sub>3</sub> composites. Densification levels from 80.6% up to 97.3% were obtained depending on the variation in scanning speed. The best result with a high relative density (RD) corresponded to a v of 550 mm/s (LED = 236 J/m), which is reasonable and optimal within the discovered processing window. Lower or higher scanning speeds decrease the densification level significantly. It should be recalled that a high volume of unmelted Al<sub>2</sub>O<sub>3</sub> regions on the depicted microstructures and a reduced densification level could be partly explained by the feedstock powder morphology features mentioned above. It is worth noting that a simple linear scan pattern was employed in this study, whereas many recent studies [91][92][93][94] showed complex strategies (such as a 67° rotation between layers and chessboard) to be more effective at obtaining a high density and porous-free material.

In a study by Han et al. [83], a Renishaw AM250 SLM machine was employed to print 8 × 8 × 8 mm<sup>3</sup> cubic samples, and a striped fill-hatch-type scanning strategy was performed with the 67° rotation between each layer. A laser power of 200 W and a scanning speed of 300 mm/s (ED<sub>v</sub> = 317.5 J/mm<sup>3</sup>) were found as optimum SLM parameters to synthesize the material with a high density of 99.49% [84]. Du et al. [76] reported the SLM of the AlSi<sub>10</sub>Mg and nAl<sub>2</sub>O<sub>3</sub> composite on the SLM 250HL machine with an 80 μm laser spot size, a layer thickness of 0.05 mm, a laser power of 350 W, a scanning speed range of 100–1500 mm/s, and a 0.1–0.2 mm hatch spacing, providing an ED<sub>v</sub> varying from 35 to 150 J/mm<sup>3</sup>. The chessboard island strategy with a 67° rotation was employed. The authors found that the use of a higher ED<sub>v</sub> (109–175

J/mm<sup>3</sup>) is appropriate for dense samples of the AlSi<sub>10</sub>Mg-nAl<sub>2</sub>O<sub>3</sub> composite, explaining it by the insulation of AlSi<sub>10</sub>Mg particles via the nAl<sub>2</sub>O<sub>3</sub> layer. In addition, an increase in composite melting pool viscosity was observed, leading to porosity defects due to the weak inter-line bonding or discontinuous melting process.

Balling phenomena [89], leading to poor interline bonding and gaps at low ED<sub>V</sub>, were observed. A higher ED<sub>V</sub> induced the porosity formation that Du et al. [76] attributed to the increased recoil pressure. Moreover, it resulted in a higher unstable melt flow and melt splashing induced by both the Marangoni convection and the recoil pressure, along with the vapor intensification [95].

Besides this, Du et al. was faced with the dynamic keyhole process, leading to pore formation during rapid solidification, inherent in the aluminum alloy with elements of low boiling points such as Si, Mn, and Mg [96]. The decrease in RD was determined not only by porosity but also by crack formation. Du et al. observed thermal shrinkage and cracks in solidified alumina along with small cavities at the edge of the nAl<sub>2</sub>O<sub>3</sub> after the low ED<sub>V</sub> SLM process. According to [63][84], an increase in ED<sub>V</sub> improves the particle–matrix interface.

The SLM of the Al-Al<sub>2</sub>O<sub>3</sub> core–shell composite with 10 wt.% of alumina prepared by the special technique described in [77] was performed by authors of a previous study [78]. The ED<sub>a</sub> of 7–8 J/mm<sup>2</sup> was found to be the optimal range for the SLM of Al-10 wt.% Al<sub>2</sub>O<sub>3</sub> core–shell powder composites, whereas the lower and higher energies caused an incomplete melting and aluminum boiling, respectively. Moreover, a lower ED insufficient for Al<sub>2</sub>O<sub>3</sub> melting led to the agglomeration at molten pool boundaries and weak bonding between the matrix and reinforcement due to the γ-Al<sub>2</sub>O<sub>3</sub> to α-Al<sub>2</sub>O<sub>3</sub> phase transition. On the contrary, the ED<sub>a</sub> increased beyond the 8 J/mm<sup>2</sup> activated deoxidation and boiling of the molten pool processes. Both incomplete melting and boiling reduced the density. The employment of ED<sub>a</sub> = 7.69 J/mm<sup>2</sup> with P = 220 W, h = 0.13, and V = 220 mm/s led to the highest sample hardness (58.3 ± 0.9 HB) and RD (96.5%). Such a relatively low RD was explained by the authors by the γ- to α-Al<sub>2</sub>O<sub>3</sub> phase transition and the particle aggregations. Further research into the double-layer exposure of the SLM mode is needed to overcome these problems. The already used and studied SLM regimes in detail are presented in Table 2.

**Table 2.** SLM parameters and RD.

Material	SLM Parameters	Maximum RD, %	Reference
Al-Al <sub>2</sub> O <sub>3</sub> 80:20 weight ratio	Spot size = 70 μm, linear raster scan pattern, P = 130 W, V = 450, 550, 650, 750 mm/s, LED = 173, 200, 236, 289 J/m	97.3	[63]
Al and 4 vol.% of Al <sub>2</sub> O <sub>3</sub>	Renishaw AM250, preheated T = 170 °C, P = 200 W, V = 100–600 mm/s (300 is optimal), t = 30 μm h = 70, 100 μm.	99.49	[84]
AlSi <sub>10</sub> Mg + 2–5wt.% nano-Al <sub>2</sub> O <sub>3</sub>	SLM 250, chessboard island strategy with a rotation of 67° at every layer. P = 350 W, V = 100–1500 mm/s, h = 0.1–0.2 mm. ED <sub>V</sub> = 35–150 J/mm <sup>3</sup> (109 is optimal)	–	[76]
Al <sub>2</sub> O <sub>3</sub> -AlSi <sub>10</sub> Mg 1:1 weight ratio	SLM-100, P = 200 W, V = 150, 200, 250, 300, and 350 mm/s(250–350 are optimal), t = 20 μm, h = 0.05, 0.1 μm (0.1 is optimal)	93	[85]
Al <sub>2</sub> O <sub>3</sub> -AlSi <sub>10</sub> Mg 15:85 weight ratio	P = 200 W, V = 100–300 mm/s, t = 20 μm, h = 60–160 μm	–	[86][87]
Al + 10 wt.% Al <sub>2</sub> O <sub>3</sub> core–shell	SLM 280 HL, P = 220 W, V = 220 mm/s, ED <sub>a</sub> = 7–8 J/mm <sup>2</sup> , h = 0.13	96.5	[78]

The casting technology proposed in [33] allowed a porosity of 1.18% to be obtained for the composite with 1% of Al<sub>2</sub>O<sub>3</sub>. The porosity increased with Al<sub>2</sub>O<sub>3</sub> content and reached more than 6% for a maximum alumina concentration of 10%. With such a complex route as stir casting with heat treatment, the addition of heat-treated particles to the melt by an inert argon gas flow could not provide a low porosity of at least less than 1%. In a previous study [41], relatively high values of RD (about 0.97) were reached only for 1 vol.% of nano-alumina after at least 150 min of sintering. The increase in both the volume fraction and particle size of alumina drastically decreased the RD. This showed the great complexity of melting and sintering approaches to produce fully dense Al-based matrix composites with Al<sub>2</sub>O<sub>3</sub> reinforcement, wherein RD < 0.99 is usually considered unsatisfactory in the SLM case. The main results of the relative densities of SLMed AMCs with Al<sub>2</sub>O<sub>3</sub> achieved in various studies are shown in Figure 3.

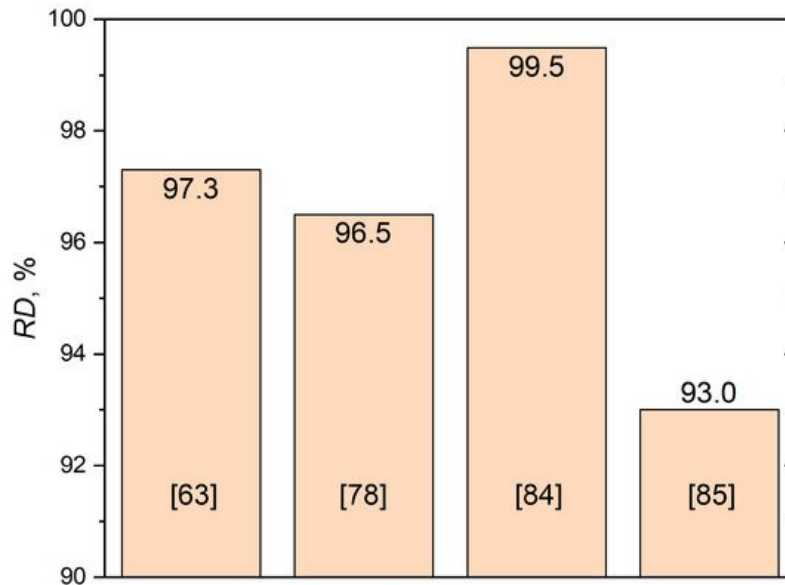


**Figure 3.** Maximum RD values of AMC + alumina materials achieved by means of the SLM technique.

It should be mentioned that there is another indirect way to obtain the Al-Al<sub>2</sub>O<sub>3</sub> composite described in [97][98]. The initial mixture of Al and 5 wt.% Fe<sub>2</sub>O<sub>3</sub> was SLMed at a laser power of 40–90 W and a scanning speed of 70–140 mm/s. The heating of the material during the melting initiated the following reaction:



Eruptive sparks were observed during the process because of the extra heat that contributed to powder melting and molten pool extension. The fine particles with a uniform distribution in the Al matrix were defined as alumina and phases of Al, Fe, and O acting as reinforcements.

Thus, it was shown that the SLM process allows the synthesis of the particles-reinforced AMC by in situ reaction. Unfortunately, there is no information about RD or any mechanical properties in that study, so it is impossible to compare the produced material with analogs.

## 4. Melting Pool Behavior

Processes within the melting pool during selective laser melting run extremely fast; hence, it is of great difficulty to study them. Some conclusions could be formulated based on the microstructural features after solidification. Jue et al. [63] showed the formation of agglomerated regions or a long-strip or ring morphology of Al<sub>2</sub>O<sub>3</sub> particles because of their displacement to the boundaries of the melting pool. The exact character of such a structure depended on the energy density of the SLM, but generally, it showed a far-from-desirable microstructure with a nonuniform distribution of reinforcing particles in the composite, which prevented the achievement of high mechanical properties (discussed in the next section). Jue et al. [63] claimed that the complete melting of the initial powder occurs, including the Al<sub>2</sub>O<sub>3</sub> phase and its formation during melting runs through the dissolution/precipitation mechanism. However, there are reasons [99][100] to believe that lower energy densities within the process window of Al-based materials via SLM do not correspond to temperatures above ~1600–1800 °C, which is lower than the alumina melting point (2044 °C); hence, the complete melting of the Al<sub>2</sub>O<sub>3</sub> phase during SLM could be achieved only at elevated energy density levels. High EDs sufficient for the melting of Al<sub>2</sub>O<sub>3</sub> could also be accompanied by undesirable processes of aluminum melt boiling (Al boiling temperature is 2519 °C), and its evaporation and emission. There are a series of studies about alumina loss during the Al-Al<sub>2</sub>O<sub>3</sub> SLM process [86][87] that shows a temperature of the melting pool higher than the alumina melting point at any set of

investigated SLM parameters. If the temperature of the molten pool is strongly influenced by the process parameters, the  $\text{Al}_2\text{O}_3$  loss phenomenon may also be controlled by the SLM regime: the setting temperature of the molten pool above the  $\text{Al}_2\text{O}_3$  melting point leads to alumina melt and resolidification; setting it above the boiling point (2977 °C) leads to alumina vaporization and loss [86]. The boiling point of Al is 2519 °C, so in the case of the temperature of the molten pool being higher than the alumina boiling point, Al will intensely burn. Thus, the presence or absence of Al loss during melting may be a marker of the molten pool temperature. In fact, no Al loss was usually observed, which means a temperature of the molten pool below 2500 °C, thus being far from the alumina boiling point. Liao et al. concluded that a notable  $\text{Al}_2\text{O}_3$  loss could not be explained by vaporization. According to Laurent et al. [62], deoxidization by the dissociative vaporization of alumina becomes noticeable only at temperatures much higher than the melting point of aluminum. Some disruption of the alumina surface could be possible in the vicinity of the Al melting point; however, it only affects a film of a few monolayers in thickness. Besides the laser power and scanning speed, hatch spacing also affects the  $\text{Al}_2\text{O}_3$  loss—the higher the hatch spacing, the lower the  $\text{Al}_2\text{O}_3$  loss. However, this dependence was observed to be nonlinear [86]—the  $\text{Al}_2\text{O}_3$  loss at a hatch spacing of 0.06 mm was smaller than that at a hatch spacing of 0.08 mm. It was explained by the difference in the laser absorptivity of the solid and powder [101], thus decreasing the temperature of the molten pool at higher overlap. According to [87], the main loss mechanism of  $\text{Al}_2\text{O}_3$  is the reduction in the reaction of  $\text{Al}_2\text{O}_3$  by aluminum. A critical temperature of 1520 °C was in the case of the  $\text{Al}_2\text{O}_3\text{-AlSi}_{10}\text{Mg}$  composite, so it was lower than the usually observed molten pool temperature under laser irradiation. Thus, notable  $\text{Al}_2\text{O}_3$  burning loss can be expected during the SLM and should be taken into account.

Returning to the temperature of the molten pool, there are some studies about the SLM/SLS of the  $\text{Al}_2\text{O}_3$  ceramic [102][103] that showed the LED values normalized to the square of the laser spot to be of the same order as those for Al-based materials melting, making the consideration about the state of alumina particles within the melting pool highly controversial. At the same time, it should be noted that, first, any discussion about reinforcing the particle distribution within the melting pool involves the presence of those particles in the solid state and, secondly, extremely high heating and cooling rates with a short lifetime of the melting pool somewhat obstruct the complete melting of  $\text{Al}_2\text{O}_3$ . Therefore, it is possible to make an assumption that the behavior of  $\text{Al}_2\text{O}_3$  particles in the melting pool may be considered as suspended solids within liquid. Based on this, the wettability of alumina by molten aluminum should be clarified. Laurent et al. [62] studied the problem and found that the contact angle  $\theta$  smoothly decreased within the range from 933 ( $\theta = 103 \pm 6^\circ$ ) to 1273 K ( $\theta = 86 \pm 6^\circ$ ), which means that the higher the temperature of the melting pool, the better the wettability.

The segregation of  $\text{Al}_2\text{O}_3$  particles during solidification is another phenomenon that should be discussed. This phenomenon arises because the  $\text{Al}_2\text{O}_3$ /solid-Al interfacial energy is higher than the  $\text{Al}_2\text{O}_3$ /liquid-Al energy [104][105], and the difference acts as a driving force, pushing alumina particles into the melt [106][107][108]. The so-called “particle pushing” results in the redistribution or segregation of the  $\text{Al}_2\text{O}_3$  particles into regions that are last to solidify.

Extremely high cooling rates inherent in SLM allow this phenomenon to be successfully avoided and allow a uniform distribution of reinforced particles to be obtained, as it was accomplished on the powder mixing/milling stage. Jue et al. [63] [80] also considered the distribution of alumina in the Al matrix specifically for SLM, taking into account the Marangoni convection and induced liquid capillary forces that accelerate the particle rearrangement, making it possible to obtain a homogeneous structure after SLM. Han et al. [84] studied the melting pool temperature during SLM with a 200 W laser power. It was observed that melting at a low scanning speed of 200 mm/s could provide the heating of the melt above the alumina melting point (2040 °C). Du et al. [76] claimed that even a higher energy input and the melting of at least some part of the  $n\text{Al}_2\text{O}_3$  could result in the increase in the  $n\text{Al}_2\text{O}_3$  particle size. In the studies of both Du et al. and Han et al.,  $\text{Al}_2\text{O}_3$  particle agglomerations were observed along the melt track edges (see [Figure 4](#)), which was explained by reinforcing particles pushing outward due to Marangoni convection and the recoil pressure.

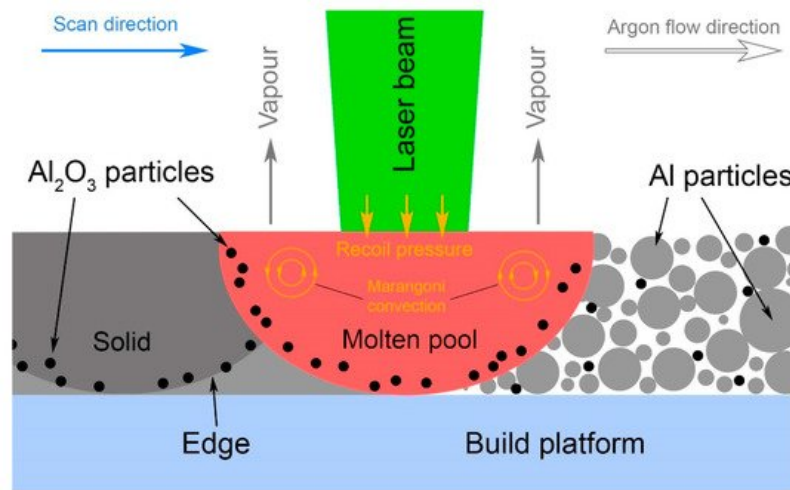


**Figure 4.** Schematic representation of reinforcing particles distribution and agglomeration along the melt track edges.

## References

1. Sahin, Y.; Murphy, S. The effect of fibre orientation of the dry sliding wear of borsic-reinforced 2014 aluminium alloy. *J. Mater. Sci.* 1996, 31, 5399–5407.
2. Seo, Y.-H.; Kang, C.-G. The effect of applied pressure on particle-dispersion characteristics and mechanical properties in melt-stirring squeeze-cast SiCp/Al composites. *J. Mater. Process. Technol.* 1995, 55, 370–379.
3. Purazrang, K.; Kainer, K.U.; Mordike, B.L. Fracture toughness behaviour of a magnesium alloy metal-matrix composite produced by the infiltration technique. *Composites* 1991, 22, 456–462.
4. Rahimian, M.; Ehsani, N.; Parvin, N.; reza Baharvandi, H. The effect of particle size, sintering temperature and sintering time on the properties of Al–Al<sub>2</sub>O<sub>3</sub> composites, made by powder metallurgy. *J. Mater. Process. Technol.* 2009, 209, 5387–5393.
5. Kok, M. Production and mechanical properties of Al<sub>2</sub>O<sub>3</sub> particle-reinforced 2024 aluminium alloy composites. *J. Mater. Process. Technol.* 2005, 161, 381–387.
6. Valiev, R.Z.; Langdon, T.G. Principles of equal-channel angular pressing as a processing tool for grain refinement. *Prog. Mater. Sci.* 2006, 51, 881–981.
7. Gu, D.D.; Meiners, W.; Wissenbach, K.; Poprawe, R. Laser additive manufacturing of metallic components: Materials, processes and mechanisms. *Int. Mater. Rev.* 2012, 57, 133–164.
8. Das, A.A.; Clegg, A.J.; Zantont, B.; Yakouh, M.M. Solidification under Pressure: Aluminium and Zinc Alloys Containing Discontinuous Sic Fibre. In *Proceedings of the Cast Reinforced MMCs*; Fishman, C.G., Dhingra, A.K., Eds.; ASM International: Materials Park, OH, USA, 1988; pp. 139–147.
9. Prasad, B.K.; Jha, A.K.; Modi, O.P.; Das, S.; Yegneswaran, A.H. Abrasive wear characteristics of Zn–37.2 Al–2.5 Cu–0.2 Mg alloy dispersed with silicon carbide particles. *Mater. Trans. JIM* 1995, 36, 1048–1057.
10. Prasad, B.K.; Das, S.; Jha, A.K.; Modi, O.P.; Dasgupta, R.; Yegneswaran, A.H. Factors controlling the abrasive wear response of a zinc-based alloy silicon carbide particle composite. *Compos. Part A Appl. Sci. Manuf.* 1997, 28, 301–308.
11. Mazahery, A.; Abdizadeh, H.; Baharvandi, H.R. Development of high-performance A356/nano-Al<sub>2</sub>O<sub>3</sub> composites. *Mater. Sci. Eng. A* 2009, 518, 61–64.
12. Torres, B.; Lieblich, M.; Ibáñez, J.; García-Escorial, A. Mechanical properties of some PM aluminide and silicide reinforced 2124 aluminium matrix composites. *Scr. Mater.* 2002, 47, 45–49.
13. Gibson, P.R.; Clegg, A.J.; Das, A.A. Production and evaluation of squeeze-cast graphitic Al–Si alloys. *Mater. Sci. Technol.* 1985, 1, 559–567.
14. Dellis, M.A.; Keustermans, J.P.; Delannay, F.; Wegria, J. ZnAl matrix composites: Investigation of the thermal expansion, creep resistance and fracture toughness. *Mater. Sci. Eng. A* 1991, 135, 253–257.
15. Rohatgi, P. Cast aluminum-matrix composites for automotive applications. *JOM* 1991, 43, 10–15.
16. Dinwoodie, J. Automotive Applications for MMC's Based on Short Staple Alumina Fibres. *SAE Trans.* 1987, 96, 269–279.

17. Joshi, S.S.; Ramakrishnan, D.; Sarathy, P.R. Development of the technology for discontinuously reinforced aluminium composites. *First World Conf. Integr. Des. Process Technol.* 1995, 1, 492–497.
18. Koczak, M.J.; Khatri, S.C.; Allison, J.E.; Bader, M.G. Metal-Matrix Composites for Ground Vehicle, Aerospace, and Industrial Applications. In *Fundamentals of Metal-Matrix Composites*; Elsevier: Amsterdam, The Netherlands, 1993; pp. 297–326. ISBN 9780080523712.
19. Chadwick, G.A.; Heath, P.J. Machining metal matrix composites. *Met. Mater. Bury St Edmunds* 1990, 2–6, 73–76.
20. Attar, H.; Prashanth, K.G.; Zhang, L.C.; Calin, M.; Okulov, I.V.; Scudino, S.; Yang, C.; Eckert, J. Effect of powder particle shape on the properties of in situ Ti-TiB composite materials produced by selective laser melting. *J. Mater. Sci. Technol.* 2015.
21. Chang, F.; Gu, D.; Dai, D.; Yuan, P. Selective laser melting of in-situ Al<sub>4</sub>SiC<sub>4</sub> + SiC hybrid reinforced Al matrix composites: Influence of starting SiC particle size. *Surf. Coatings Technol.* 2015.
22. Surappa, M.K.; Prasad, S.V.; Rohatgi, P.K. Wear and abrasion of cast Al-Alumina particle composites. *Wear* 1982.
23. Purohit, R.; Qureshi, M.M.U.; Jain, A. Forming behaviour of aluminium matrix nano Al<sub>2</sub>O<sub>3</sub> composites for automotive applications. *Adv. Mater. Process. Technol.* 2020, 6, 272–283.
24. Singh, J.; Chauhan, A. Overview of wear performance of aluminium matrix composites reinforced with ceramic materials under the influence of controllable variables. *Ceram. Int.* 2016, 42, 56–81.
25. Rahimian, M.; Parvin, N.; Ehsani, N. The effect of production parameters on microstructure and wear resistance of powder metallurgy Al-Al<sub>2</sub>O<sub>3</sub> composite. *Mater. Des.* 2011, 32, 1031–1038.
26. Park, B.G.; Crosky, A.G.; Hellier, A.K. Material characterisation and mechanical properties of Al<sub>2</sub>O<sub>3</sub>-Al metal matrix composites. *J. Mater. Sci.* 2001, 36, 2417–2426.
27. Dobrzański, L.A.; Włodarczyk, A.; Adamiak, M. The structure and properties of PM composite materials based on EN AW-2124 aluminum alloy reinforced with the BN or Al<sub>2</sub>O<sub>3</sub> ceramic particles. *J. Mater. Process. Technol.* 2006, 175, 186–191.
28. Prashanth, K.G.; Scudino, S.; Chaubey, A.K.; Löber, L.; Wang, P.; Attar, H.; Schimansky, F.P.; Pyczak, F.; Eckert, J. Processing of Al-12Si-TiN composites by selective laser melting and evaluation of compressive and wear properties. *J. Mater. Res.* 2016.
29. Shorowordi, K.M.; Laoui, T.; Haseeb, A.S.M.A.; Celis, J.P.; Froyen, L. Microstructure and interface characteristics of B<sub>4</sub>C, SiC and Al<sub>2</sub>O<sub>3</sub> reinforced Al matrix composites: A comparative study. *J. Mater. Process. Technol.* 2003, 142, 738–743.
30. Sahin, Y.; Kok, M.; Celik, H. Tool wear and surface roughness of Al<sub>2</sub>O<sub>3</sub> particle-reinforced aluminium alloy composites. *J. Mater. Process. Technol.* 2002, 128, 280–291.
31. Singh, J.; Chauhan, A. Characterization of hybrid aluminum matrix composites for advanced applications—A review. *J. Mater. Res. Technol.* 2016, 5, 159–169.
32. Yadav, S.; Chichili, D.R.; Ramesh, K.T. The mechanical response of a 6061-T6 Al<sub>1</sub>/Al<sub>2</sub>O<sub>3</sub> metal matrix composite at high rates of deformation. *Acta Metall. Mater.* 1995, 43, 4453–4464.
33. Sajjadi, S.A.; Ezatpour, H.R.; Beygi, H. Microstructure and mechanical properties of Al–Al<sub>2</sub>O<sub>3</sub> micro and nano composites fabricated by stir casting. *Mater. Sci. Eng. A* 2011, 528, 8765–8771.
34. Hanumanth, G.S.; Irons, G.A. Particle incorporation by melt stirring for the production of metal-matrix composites. *J. Mater. Sci.* 1993, 28, 2459–2465.
35. Taha, M.A.; El-Mahallawy, N.A. Metal–matrix composites fabricated by pressure-assisted infiltration of loose ceramic powder. *J. Mater. Process. Technol.* 1998, 73, 139–146.
36. Rosso, M. Ceramic and metal matrix composites: Routes and properties. *J. Mater. Process. Technol.* 2006, 175, 364–375.
37. Lafreniere, S.; Irons, G.A. Sedimentation During Liquid Processing of Metal Matrix Composites. In *Production, Refining, Fabrication and Recycling of Light Metals*; Elsevier: Amsterdam, The Netherlands, 1990; pp. 177–186.
38. Ibrahim, I.A.; Mohamed, F.A.; Lavernia, E.J. Particulate reinforced metal matrix composites—A review. *J. Mater. Sci.* 1991, 26, 1137–1156.
39. Banerji, A.; Rohatgi, P.K.; Reif, W. Role of Wettability in The Preparation of Metal-Matrix Composites (A Review). *Metall* 1984, 38, 656–661.
40. Asthana, R.; Rohatgi, P.K. On the melt infiltration of copper coated silicon carbide with an aluminium alloy. *Compos. Manuf.* 1992, 3, 119–123.

41. Razavi-Tousi, S.S.; Yazdani-Rad, R.; Manafi, S.A. Effect of volume fraction and particle size of alumina reinforcement on compaction and densification behavior of Al–Al<sub>2</sub>O<sub>3</sub> nanocomposites. *Mater. Sci. Eng. A* 2011, 528, 1105–1110.
42. Rahimian, M.; Parvin, N.; Ehsani, N. Investigation of particle size and amount of alumina on microstructure and mechanical properties of Al matrix composite made by powder metallurgy. *Mater. Sci. Eng. A* 2010, 527, 1031–1038.
43. Sevik, H.; Kurnaz, S.C. Properties of alumina particulate reinforced aluminum alloy produced by pressure die casting. *Mater. Des.* 2006, 27, 676–683.
44. Lloyd, D.J. Particle reinforced aluminium and magnesium matrix composites. *Int. Mater. Rev.* 1994, 39, 1–23.
45. Zebarjad, S.M.; Sajjadi, S.A. Dependency of physical and mechanical properties of mechanical alloyed Al–Al<sub>2</sub>O<sub>3</sub> composite on milling time. *Mater. Des.* 2007, 28, 2113–2120.
46. Zhou, W.; Xu, Z.M. Casting of SiC reinforced metal matrix composites. *J. Mater. Process. Technol.* 1997, 63, 358–363.
47. Lewandowski, J.J.; Seifi, M. Metal Additive Manufacturing: A Review of Mechanical Properties. *Annu. Rev. Mater. Res.* 2016, 46, 151–186.
48. Read, N.; Wang, W.; Essa, K.; Attallah, M.M. Selective laser melting of AlSi10Mg alloy: Process optimisation and mechanical properties development. *Mater. Des.* 2015, 65, 417–424.
49. Aboulkhair, N.T.; Simonelli, M.; Parry, L.; Ashcroft, I.; Tuck, C.; Hague, R. 3D printing of Aluminium alloys: Additive Manufacturing of Aluminium alloys using selective laser melting. *Prog. Mater. Sci.* 2019, 106, 100578.
50. Gu, D.; Wang, H.; Dai, D.; Yuan, P.; Meiners, W.; Poprawe, R. Rapid fabrication of Al-based bulk-form nanocomposites with novel reinforcement and enhanced performance by selective laser melting. *Scr. Mater.* 2015, 96, 25–28.
51. Yuan, P.; Gu, D.; Dai, D. Particulate migration behavior and its mechanism during selective laser melting of TiC reinforced Al matrix nanocomposites. *Mater. Des.* 2015, 82, 46–55.
52. Sercombe, T.B.; Li, X. Selective laser melting of aluminium and aluminium metal matrix composites: Review. *Mater. Technol.* 2016, 31, 77–85.
53. Wang, P.; Gammer, C.; Brenne, F.; Niendorf, T.; Eckert, J.; Scudino, S. A heat treatable TiB<sub>2</sub>/Al-3.5Cu-1.5Mg-1Si composite fabricated by selective laser melting: Microstructure, heat treatment and mechanical properties. *Compos. Part B Eng.* 2018, 147, 162–168.
54. Dieter, G.E. *Mechanical Metallurgy*, 3rd ed.; McGraw-Hill: New York, NY, USA, 1976.
55. Gu, D.; Yuan, P. Thermal evolution behavior and fluid dynamics during laser additive manufacturing of Al-based nanocomposites: Underlying role of reinforcement weight fraction. *J. Appl. Phys.* 2015, 118, 233109.
56. Li, R.; Liu, J.; Shi, Y.; Wang, L.; Jiang, W. Balling behavior of stainless steel and nickel powder during selective laser melting process. *Int. J. Adv. Manuf. Technol.* 2012, 59, 1025–1035.
57. Gu, D. *Laser Additive Manufacturing of High-Performance Materials*; Springer: Berlin/Heidelberg, Germany, 2015; ISBN 9783662460894.
58. Dadbakhsh, S.; Hao, L.; Jerrard, P.G.E.; Zhang, D.Z. Experimental investigation on selective laser melting behaviour and processing windows of in situ reacted Al/Fe<sub>2</sub>O<sub>3</sub> powder mixture. *Powder Technol.* 2012, 231, 112–121.
59. Zhang, B.; Liao, H.; Coddet, C. Effects of processing parameters on properties of selective laser melting Mg-9%Al powder mixture. *Mater. Des.* 2012, 34, 753–758.
60. McCoy, J.W.; Franklin, E.W. Dendritic Segregation in Particle Reinforced Cast Aluminium Composites. In *Cast Reinforced Metal Composites*; Fishman, S.G., Dhingra, A.K., Eds.; ASM: Metals Park, OH, USA; Chicago, IL, USA, 1988; pp. 77–80.
61. Khairallah, S.A.; Anderson, A.T.; Rubenchik, A.; King, W.E. Laser powder-bed fusion additive manufacturing: Physics of complex melt flow and formation mechanisms of pores, spatter, and denudation zones. *Acta Mater.* 2016, 108, 36–45.
62. Laurent, V.; Chatain, D.; Chatillon, C.; Eustathopoulos, N. Wettability of monocrystalline alumina by aluminium between its melting point and 1273 K. *Acta Metall.* 1988, 36, 1797–1803.
63. Jue, J.; Gu, D.; Chang, K.; Dai, D. Microstructure evolution and mechanical properties of Al–Al<sub>2</sub>O<sub>3</sub> composites fabricated by selective laser melting. *Powder Technol.* 2017, 310, 80–91.
64. Suryanarayana, C. Mechanical alloying and milling. *Prog. Mater. Sci.* 2001, 46, 1–184.
65. Sommer, M.; Stenger, F.; Peukert, W.; Wagner, N.J. Agglomeration and breakage of nanoparticles in stirred media mills—a comparison of different methods and models. *Chem. Eng. Sci.* 2006, 61, 135–148.
66. Han, Q.; Setchi, R.; Evans, S.L. Synthesis and characterisation of advanced ball-milled Al–Al<sub>2</sub>O<sub>3</sub> nanocomposites for selective laser melting. *Powder Technol.* 2016, 297, 183–192.

67. Olakanmi, E.O. Selective laser sintering/melting (SLS/SLM) of pure Al, Al–Mg, and Al–Si powders: Effect of processing conditions and powder properties. *J. Mater. Process. Technol.* 2013, 213, 1387–1405.
68. Han, Q.; Setchi, R.; Evans, S.L. Characterisation and milling time optimisation of nanocrystalline aluminium powder for selective laser melting. *Int. J. Adv. Manuf. Technol.* 2017, 88, 1429–1438.
69. To, D.; Dave, R.; Yin, X.; Sundaresan, S. Deagglomeration of nanoparticle aggregates via rapid expansion of supercritical or high-pressure suspensions. *AIChE J.* 2009, 55, 2807–2826.
70. Friedlander, S.K.; Marlow, W.H. *Smoke, Dust and Haze: Fundamentals of Aerosol Behavior.* *Phys. Today* 1977, 30, 58–59.
71. Nam, C.H.; Pfeffer, R.; Dave, R.N.; Sundaresan, S. Aerated vibrofluidization of silica nanoparticles. *AIChE J.* 2004.
72. Yu, Q.; Dave, R.N.; Zhu, C.; Quevedo, J.A.; Pfeffer, R. Enhanced fluidization of nanoparticles in an oscillating magnetic field. *AIChE J.* 2005, 51, 1971–1979.
73. Kurkela, J.A.; Brown, D.P.; Raula, J.; Kauppinen, E.I. New apparatus for studying powder deagglomeration. *Powder Technol.* 2008, 180, 164–171.
74. Yao, W.; Guangsheng, G.; Fei, W.; Jun, W. Fluidization and agglomerate structure of SiO<sub>2</sub> nanoparticles. *Powder Technol.* 2002, 124, 152–159.
75. Van Der Wel, P. Powder mixing. *Powder Handl. Process.* 1999, 11, 83–86.
76. Du, Z.; Chen, H.C.; Tan, M.J.; Bi, G.; Chua, C.K. Effect of nAl<sub>2</sub>O<sub>3</sub> on the part density and microstructure during the laser-based powder bed fusion of AlSi10Mg composite. *Rapid Prototyp. J.* 2020, 26, 727–735.
77. Gromov, A.A.; Nalivaiko, A.Y.; Ambaryan, G.N.; Vlaskin, M.S.; Buryakovskaya, O.A.; Kislenco, S.A.; Zhuk, A.Z.; Shkolnikov, E.I.; Slyusarskiy, K.V.; Osipenkova, A.A.; et al. Aluminum-alumina composites: Part I: Obtaining and characterization of powders. *Materials* 2019, 12, 3180.
78. Nalivaiko, A.Y.; Ozherelkov, D.Y.; Arnautov, A.N.; Zmanovsky, S.V.; Osipenkova, A.A.; Gromov, A.A. Selective laser melting of aluminum-alumina powder composites obtained by hydrothermal oxidation method. *Appl. Phys. A Mater. Sci. Process.* 2020, 126, 1–6.
79. Nalivaiko, A.Y.; Arnautov, A.N.; Zmanovsky, S.V.; Ozherelkov, D.Y.; Shurkin, P.K.; Gromov, A.A. Al–Al<sub>2</sub>O<sub>3</sub> powder composites obtained by hydrothermal oxidation method: Powders and sintered samples characterization. *J. Alloys Compd.* 2020, 825, 154024.
80. Wang, L.; Jue, J.; Xia, M.; Guo, L.; Yan, B.; Gu, D. Effect of the thermodynamic behavior of selective laser melting on the formation of in situ oxide dispersion-strengthened aluminum-based composites. *Metals* 2016, 6, 286.
81. Gu, D.; Jue, J.; Dai, D.; Lin, K.; Chen, W. Effects of Dry Sliding Conditions on Wear Properties of Al-Matrix Composites Produced by Selective Laser Melting Additive Manufacturing. *J. Tribol.* 2018, 140, 021605.
82. Jue, J.; Gu, D. Selective laser melting additive manufacturing of in situ Al<sub>2</sub>Si<sub>4</sub>O<sub>10</sub>/Al composites: Microstructural characteristics and mechanical properties. *J. Compos. Mater.* 2017.
83. Han, Q.; Geng, Y.; Setchi, R.; Lacan, F.; Gu, D.; Evans, S.L. Macro and nanoscale wear behaviour of Al–Al<sub>2</sub>O<sub>3</sub> nanocomposites fabricated by selective laser melting. *Compos. Part B Eng.* 2017, 127, 26–35.
84. Han, Q.; Setchi, R.; Lacan, F.; Gu, D.; Evans, S.L. Selective laser melting of advanced Al–Al<sub>2</sub>O<sub>3</sub> nanocomposites: Simulation, microstructure and mechanical properties. *Mater. Sci. Eng. A* 2017, 698, 162–173.
85. Liao, H.; Zhu, H.; Zhu, J.; Chang, S.; Zeng, X. Effect of Process Parameters on Selective Laser Melting Al<sub>2</sub>O<sub>3</sub>–Al Ceramic Material. In *Proceedings of the Solid Freeform Fabrication Symposium—An Additive Manufacturing Conference*, Austin, TX, USA, 12–14 August 2019.
86. Liao, H.; Zhu, H.; Xue, G.; Zeng, X. Alumina loss mechanism of Al<sub>2</sub>O<sub>3</sub>–AlSi<sub>10</sub> Mg composites during selective laser melting. *J. Alloys Compd.* 2019, 785, 286–295.
87. Liao, H.; Zhu, J.; Chang, S.; Xue, G.; Zhu, H.; Chen, B. Al<sub>2</sub>O<sub>3</sub> loss prediction model of selective laser melting Al<sub>2</sub>O<sub>3</sub>–Al composite. *Ceram. Int.* 2020, 46, 13414–13423.
88. Oliveira, J.P.; LaLonde, A.D.; Ma, J. Processing parameters in laser powder bed fusion metal additive manufacturing. *Mater. Des.* 2020, 193, 108762.
89. Gu, D.; Wang, H.; Chang, F.; Dai, D.; Yuan, P.; Hagedorn, Y.-C.; Meiners, W. Selective Laser Melting Additive Manufacturing of TiC/AlSi<sub>10</sub>Mg Bulk-form Nanocomposites with Tailored Microstructures and Properties. *Phys. Procedia* 2014, 56, 108–116.
90. Roberts, I.A.; Wang, C.J.; Esterlein, R.; Stanford, M.; Mynors, D.J. A three-dimensional finite element analysis of the temperature field during laser melting of metal powders in additive layer manufacturing. *Int. J. Mach. Tools Manuf.* 2009,

91. Cheng, B.; Shrestha, S.; Chou, K. Stress and deformation evaluations of scanning strategy effect in selective laser melting. *Addit. Manuf.* 2016, 12, 240–251.
92. Koutny, D.; Palousek, D.; Pantelejev, L.; Hoeller, C.; Pichler, R.; Tesicky, L.; Kaiser, J. Influence of scanning strategies on processing of aluminum alloy EN AW 2618 using selective laser melting. *Materials* 2018, 11, 298.
93. Dai, D.; Gu, D.; Zhang, H.; Xiong, J.; Ma, C.; Hong, C.; Poprawe, R. Influence of scan strategy and molten pool configuration on microstructures and tensile properties of selective laser melting additive manufactured aluminum based parts. *Opt. Laser Technol.* 2018, 99, 91–100.
94. Sun, S.H.; Hagihara, K.; Nakano, T. Effect of scanning strategy on texture formation in Ni-25 at.%Mo alloys fabricated by selective laser melting. *Mater. Des.* 2018, 140, 307–316.
95. Liu, Y.; Yang, Y.; Mai, S.; Wang, D.; Song, C. Investigation into spatter behavior during selective laser melting of AISI 316L stainless steel powder. *Mater. Des.* 2015, 87, 797–806.
96. Miyagi, M.; Wang, H.; Yoshida, R.; Kawahito, Y.; Kawakami, H.; Shoubu, T. Effect of alloy element on weld pool dynamics in laser welding of aluminum alloys. *Sci. Rep.* 2018, 8, 12944.
97. Dadbakhsh, S.; Hao, L. In situ formation of particle reinforced Al matrix composite by selective laser melting of Al/Fe<sub>2</sub>O<sub>3</sub> powder mixture. *Adv. Eng. Mater.* 2012, 14, 45–48.
98. Dadbakhsh, S.; Hao, L. Effect of Al alloys on selective laser melting behaviour and microstructure of in situ formed particle reinforced composites. *J. Alloys Compd.* 2012, 541, 328–334.
99. Yuan, P.; Gu, D. Molten pool behaviour and its physical mechanism during selective laser melting of TiC/AISI10Mg nanocomposites: Simulation and experiments. *J. Phys. D Appl. Phys.* 2015, 48, 035303.
100. Li, Y.; Gu, D. Parametric analysis of thermal behavior during selective laser melting additive manufacturing of aluminum alloy powder. *Mater. Des.* 2014, 63, 856–867.
101. Gusarov, A.V. Radiation transfer in metallic-powder beds during laser forming. *Quantum Electron.* 2010, 40, 451.
102. Fan, Z.; Lu, M.; Huang, H. Selective laser melting of alumina: A single track study. *Ceram. Int.* 2018, 44, 9484–9493.
103. Fayed, E.M.; Elmesalamy, A.S.; Sobih, M.; Elshaer, Y. Characterization of direct selective laser sintering of alumina. *Int. J. Adv. Manuf. Technol.* 2018, 94, 2333–2341.
104. Yu, P.; Deng, C.-J.; Ma, N.-G.; Ng, D.H.L. A new method of producing uniformly distributed alumina particles in Al-based metal matrix composite. *Mater. Lett.* 2004, 58, 679–682.
105. Mortensen, A.; Jin, I. Solidification processing of metal matrix composites. *Int. Mater. Rev.* 1992, 37, 101–128.
106. Uhlmann, D.R.; Chalmers, B.; Jackson, K.A. Interaction Between Particles and a Solid-Liquid Interface. *J. Appl. Phys.* 1964, 35, 2986–2993.
107. Cissé, J.; Bolling, G.F. A study of the trapping and rejection of insoluble particles during the freezing of water. *J. Cryst. Growth* 1971, 10, 67–76.
108. Omenyi, S.N.; Neumann, A.W. Thermodynamic aspects of particle engulfment by solidifying melts. *J. Appl. Phys.* 1976, 43, 727–732.